

Ferromagnetic - spin glass transition induced by pressure in the geometrically frustrated pyrochlore $(\text{Tb}_{1-x}\text{La}_x)_2\text{Mo}_2\text{O}_7$

A. Apetrei¹, I. Mirebeau¹, I. Goncharenko¹, D. Andreica^{2,3} and P. Bonville⁴

¹*Laboratoire Léon Brillouin, CEA-CNRS, CE-Saclay, 91191 Gif-sur-Yvette, France*

²*Laboratory for Muon-Spin Spectroscopy, Paul Scherrer Institut, 5232 Villigen-PSI, Switzerland*

³*Babes-Bolyai University, Faculty of Physics, 400084 Cluj-Napoca, Romania and*

⁴*Service de Physique de l'Etat Condensé, CEA-CNRS, CE-Saclay, 91191 Gif-Sur-Yvette, France*

We have studied $(\text{Tb}_{1-x}\text{La}_x)_2\text{Mo}_2\text{O}_7$ pyrochlores by neutron diffraction and μSR at ambient and under applied pressure. Substitution of Tb for La expands the lattice and induces a change from a spin-glass like state ($x=0$) to a non collinear ferromagnet ($x=0.2$). In the ferromagnetic structure, the Tb moments orient close to their local anisotropy axis as for an ordered spin ice, while the Mo moments orient close to the net moment. The μSR dynamical relaxation rate shows a cusp-like peak at the Curie temperature T_C and a broad anomaly at $T^* < T_C$, suggesting a second transition of local or dynamical nature. Under pressure, the long range order breaks down and a spin glass-like state is recovered. The whole set of data provide a microscopic picture of the spin correlations and fluctuations in the region of the ferromagnetic-spin glass threshold.

PACS numbers: 71.30.+h, 71.27.+a, 75.25.+z

In the pyrochlore compounds $\text{R}_2\text{Mo}_2\text{O}_7$, both rare earth R^{3+} and M^{4+} transition metal form a three-dimensional network of corner sharing tetrahedra. The pyrochlore lattice is geometrically frustrated for antiferromagnetic (AF) nearest-neighbour exchange interactions between Heisenberg spins. It is also frustrated for ferromagnetic (F) interactions if spins are constrained along their local anisotropy axes. Geometrical frustration can lead to intriguing short range ordered phases with ground state degeneracy, such as spin liquids, spin ices or chemically ordered spin glasses^{1,2}.

$\text{R}_2\text{Mo}_2\text{O}_7$ pyrochlores were extensively studied since their electrical and magnetic properties exhibit an unusual variation with the rare earth ionic radius r . Compounds with small ionic radius $\text{R} = \text{Y}, \text{Dy}$ and Tb show spin glass (SG) insulating behaviour, whereas those with $\text{R} = \text{Gd}, \text{Sm}$ and Nd show ferromagnetic (F) metallic behaviour. $(\text{RR}')_2\text{Mo}_2\text{O}_7$ series with different substitutions on the R^{3+} site show a universal dependence of the magnetic transition temperature on the average R^{3+} ionic radius^{3,4}. It suggests that the sign of Mo-Mo interactions controls the formation of the spin glass/ferromagnetic state. Photoemission experiments and band structure calculations^{5,6} point out that the concomitant changes of the transport and magnetic properties come from strong electron correlations in the $\text{Mo}(t_{2g})$ band nearby the Fermi level.

Few microscopic studies of the magnetic order and spin fluctuations were performed up to now in $\text{R}_2\text{Mo}_2\text{O}_7$. They all deal with compounds far from the threshold ionic radius r_c between SG and F regions. $\text{Y}_2\text{Mo}_2\text{O}_7$ and $\text{Tb}_2\text{Mo}_2\text{O}_7$ with $r < r_c$ were thoroughly investigated^{7,8,9,10}, since the occurrence of a SG transition is surprising with regards to their chemical order. On the F side, $\text{Nd}_2\text{Mo}_2\text{O}_7$ with $r > r_c$ was also intensively studied^{11,12} due to its giant abnormal Hall effect. F compounds nearby the threshold ($\text{R} = \text{Sm}, \text{Gd}$) are difficult to study since they strongly absorb neutrons. The study

of mixed $(\text{RR}')_2\text{Mo}_2\text{O}_7$ compounds near the threshold is also intricate since three magnetic ions are involved. Therefore neither the role of R^{3+} magnetism nor the evolution of the spin correlations and fluctuations near the threshold have been clarified so far.

To understand the role of interatomic distances in the SG-F transition, the most direct way is to combine applied pressure and chemical pressure. This is done here in a single and "simple" system $(\text{Tb}_{1-x}\text{La}_x)_2\text{Mo}_2\text{O}_7$, studied by neutron diffraction and μSR at ambient and applied pressure. Substitution of Tb for La expands the lattice, encompassing the threshold for a small La content ($x \sim 0.06$) which does not perturb much the Tb lattice, since La is not magnetic. By neutron diffraction, we follow the evolution of the spin correlation from SG to F state at a microscopic level. For $x=0.2$ we observe a new ordered magnetic structure, involving non collinear ferromagnetic arrangement of both Tb- and Mo- moments. Under pressure the $x=0.2$ sample transforms into a spin glass similar to $\text{Tb}_2\text{Mo}_2\text{O}_7$, showing the equivalence of chemical and applied pressures. While neutron diffraction probes magnetic correlations, μSR measurements allows us to study spin fluctuations. For $x=0.2$, we observe by μSR a second transition well below the Curie transition. The two transitions seem to merge with increasing pressure. The whole data provide a fully new picture of the F-SG threshold.

The crystal structure of $(\text{Tb}_{1-x}\text{La}_x)_2\text{Mo}_2\text{O}_7$ powders ($x=0, 0.05, 0.1, 0.15, 0.2$) was characterized at 300 K by combining X-ray and neutron diffraction. Rietveld refinements performed with FULLPROF¹³ show that all samples crystallize in $Fd\bar{3}m$ cubic space group, with a lattice constant a between 10.312 Å ($x=0$) and 10.378 Å ($x=0.2$). The $x=0.10$ sample ($a=10.346$ Å) is above the critical threshold ($a_c=10.332$ Å). The lattice constant was measured under pressure for $x=0$ and 0.2 on the ID27 beam line of the European Synchrotron Radiation Facility (ESRF). Susceptibility data show an evolution

between a spin glass state ($x=0$) characterized by irreversibilities of field-cooled/zero field-cooled curves below $T_{SG} \sim 22$ K and a ferromagnetic state ($x=0.2$) indicated by a strong increase of magnetization below $T_C \sim 58$ K.

Magnetic diffraction patterns at ambient pressure were recorded on the powder diffractometers G61 and G41 of the Laboratoire Léon Brillouin (LLB) in the temperature range 1.4 K - 100 K. High pressure neutron diffraction patterns were recorded on G61 in the high pressure version¹⁴. The neutron diffraction patterns show the evolution of the magnetic order when going through the critical threshold by substitution of Tb for La (Fig. 1a) and by applied pressure (Fig. 1b). It is a clear evidence that magnetic changes induced by chemical and applied pressures are equivalent.

In $\text{Tb}_2\text{Mo}_2\text{O}_7$ ($x=0$) short range correlations yield diffuse maxima around $q = 1$ and 2 \AA^{-1} . An intense signal at low q values shows the presence of ferromagnetic correlations. For $x=0.10$, Lorentzian peaks start to grow at the position of the diffuse maxima, revealing the onset of mesoscopic magnetic order. For $x=0.2$, the low q signal almost disappears and we clearly see magnetic Bragg peaks showing long range magnetic order. When we apply pressure on the $x=0.2$ sample, the intensity of the Bragg peaks decreases and the ferromagnetic correlations and diffuse maxima start to grow. The magnetic pattern for $x=0.2$ at 1.05 GPa (resp 3.7 GPa) is very similar to that for $x=0.10$ (resp $x=0$) at ambient pressure.

In the range $q = 0.5\text{--}2.5 \text{ \AA}^{-1}$, we analyzed the magnetic correlations in $\text{Tb}_2\text{Mo}_2\text{O}_7$ by a short range magnetic model in the same way as in Ref. 8. A fit of the diffuse magnetic intensity by the sum of radial correlation functions was performed, giving information on spin-spin correlation parameters γ up to the fourth coordination shell ($\sim 7.3 \text{ \AA}$). The Tb-Tb correlations are F ($\gamma_{1,3,4} > 0$), while the Tb-Mo are AF ($\gamma_2 < 0$) in agreement with previous results⁸. The AF Mo-Mo correlations responsible for the frustration in the SG state¹⁰ cannot be detected, their contribution being about 50 times smaller than the Tb-Tb ones due to the smaller Mo moment. The intense signal below 0.5 \AA^{-1} was not detected in previous patterns measured in a higher q range^{8,9}. It cannot be accounted for by the short range magnetic model, even when increasing the correlation range up to the seventh coordination shell. We attribute this signal to ferromagnetic correlations between Tb moments. We evaluate their lengthscale to about 20 \AA .

The magnetic Bragg peaks observed for $x=0.2$ belong to the face centered cubic lattice, showing that the magnetic structure is derived from the chemical structure of $Fd\bar{3}m$ symmetry by a propagation vector $\mathbf{k}=0$. The presence of two magnetic peaks (200) and (220) forbidden in the pyrochlore structure suggests a non-collinear F structure.

To study the spin arrangement precisely, Rietveld refinements of the magnetic diffraction patterns (Fig. 2) were performed with FULLPROF¹³. The magnetic structure was solved by a systematic search, us-

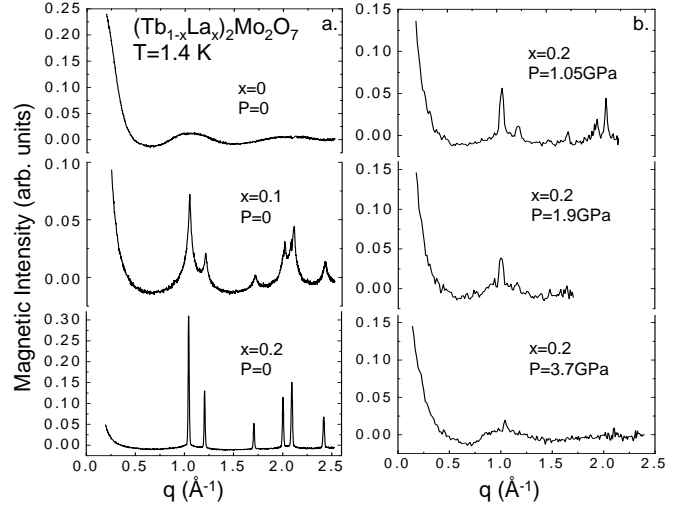


FIG. 1: Magnetic intensity of $(\text{Tb}_{1-x}\text{La}_x)_2\text{Mo}_2\text{O}_7$ at 1.4 K versus the scattering vector $q=4\pi\sin\theta/\Lambda$. The neutron wavelength is $\Lambda = 4.741 \text{ \AA}$. A spectrum in the paramagnetic phase (70 K) was subtracted and the magnetic intensity was scaled to the (222) nuclear peak intensity.

ing the program BasIreps¹⁵ and symmetry-representation analysis¹⁶. Since neither a collinear F structure nor the $\mathbf{k}=0$ AF structure allowed by $Fd\bar{3}m$ symmetry were compatible with the experimental data, we searched for a solution in the space group $I4_1/amd$, the highest subgroup allowing F and AF components simultaneously. The best refinement ($R_B = 4 \%$) is shown in Fig. 2a. In the ordered structure with $\mathbf{k}=0$, the four tetrahedra of the unit cell are equivalent, for both the Tb and Mo lattices. In a given Tb tetrahedron (inset Fig. 2a), the Tb^{3+} magnetic moments make an angle $\theta_t = 11.6^\circ$ at 1.4 K with the local $\langle 111 \rangle$ anisotropy axes connecting the center to the vertices. The components along these $\langle 111 \rangle$ axes are oriented in the "two in, two out" configuration of the local spin ice structure¹. The F component orders along a $[001]$ axis. The Mo moments align close to a $[001]$ axis (inset Fig. 2a), with a slight tilting by the angle $\theta_m = 6.8^\circ$ at 1.4 K towards the local $\langle 111 \rangle$ axes. In this structure, both Mo-Mo and Tb-Mo correlations are F, in contrast with the spin glass described above. Interestingly for $T < 40$ K a diffuse intensity shows the onset of short range correlations. These correlations coexist with the long range order, have the same symmetry and their intensity increases with decreasing temperature. A full description will be given in a future paper.

Figure 2b shows the variation of Tb and Mo magnetic moments with temperature. Below 40 K M_{Mo} is almost T-independent, while M_{Tb} keeps increasing below T_C . The ordered moments at 1.4 K, $M_{\text{Tb}} = 4.66(1) \mu_B$ and $M_{\text{Mo}} = 0.64(2) \mu_B$ are well reduced from the free ion values of $9 \mu_B$ and $2 \mu_B$, respectively. For Tb, this strong reduction could be mainly explained by crystal field effects. As for Mo, it could arise from a band effect and/or quantum fluctuations. The two tilting angles slightly de-

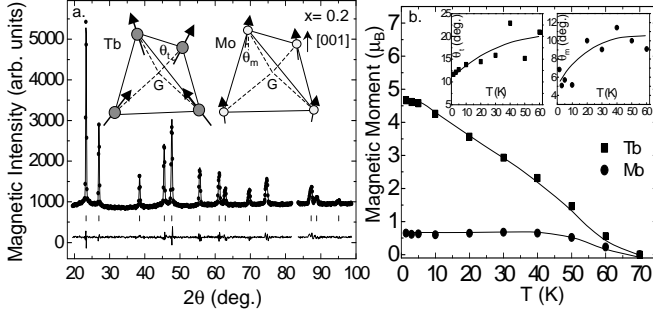


FIG. 2: a. Magnetic intensity in the $x=0.2$ sample at 1.5 K versus the scattering angle 2θ , with $\Lambda=2.426$ Å. A spectrum at 70 K was subtracted. Solid lines show the best refinement ($R_B=4\%$) and the difference spectrum (bottom). In the inset the magnetic structure of the Tb- and Mo-tetrahedra. b. Ordered magnetic moments versus temperature. In inset the angles θ_t and θ_m made by Tb- and Mo- moments with the local anisotropy $\langle 111 \rangle$ and the $[001]$ axes, respectively. Solid lines are guides to the eye.

crease with decreasing temperature (inset Fig. 2b).

The obtained non collinear structure both for Tb^{3+} and Mo^{4+} originates from the uniaxial anisotropy of the Tb^{3+} ion, which brings spin ice frustration to the ferromagnetic phase. The ground state is determined by Mo-Mo F exchange interactions like in $\text{Nd}_2\text{Mo}_2\text{O}_7$ ¹¹, while in the "ordered spin ice" $\text{Tb}_2\text{Sn}_2\text{O}_7$ with similar orientation of Tb^{3+} moments¹⁷ it results from F dipolar interactions between the Tb^{3+} ions.

Under pressure, the ordered moments ($x=0.2$) decrease and reorient (Fig. 3). For $P=1.05$ GPa, we observed the coexistence of long and short range ordered phases of the same symmetry, yielding Bragg peaks and a diffuse background respectively. The ordered Tb moments keep the "two in, two out" spin configurations with a different $\theta'_t = 28.3^\circ$, while the Mo ones turn to a local spin ice structure, making an angle $\theta'_m = 7.3^\circ$ with the local $\langle 111 \rangle$ axes. At 3.7 GPa the Bragg peak disappear. The near-neighbour correlations parameters are similar to those of $\text{Tb}_2\text{Mo}_2\text{O}_7$: F Tb-Tb correlations ($\gamma_{1,3,4} > 0$) and AF Tb-Mo correlations ($\gamma_2 < 0$). The ferromagnetic correlation length of 18 Å is also similar. The ordering temperature decreases with increasing pressure.

μSR measurements (Fig. 4) shed a new light on the magnetic order by probing the spin fluctuations and the static local field below T_C . The recent availability of μSR under pressure allows us to probe them on both sides of the threshold. We measured the $x=0.2$ sample at ambient pressure on the GPS and GPD instruments of the Paul Scherrer Institut (PSI) and under a pressure of 1.3 GPa on GPD. The muon spin depolarization function $P_Z(t)$ for several spectra recorded at ambient pressure is shown in Fig 4a.

μSR spectra above T_C were best fitted with a stretched exponential function $P_Z(t) = \exp(-\lambda t)^\beta$. Below T_C , $P_Z(t)$ was fitted by the function $P_Z(t) = [\exp(-\lambda_Z t)^\beta + 2 \exp(-\lambda_T t) \cos(\gamma_\mu \langle B_{loc} \rangle t)]/3$, expected for the the magneti-

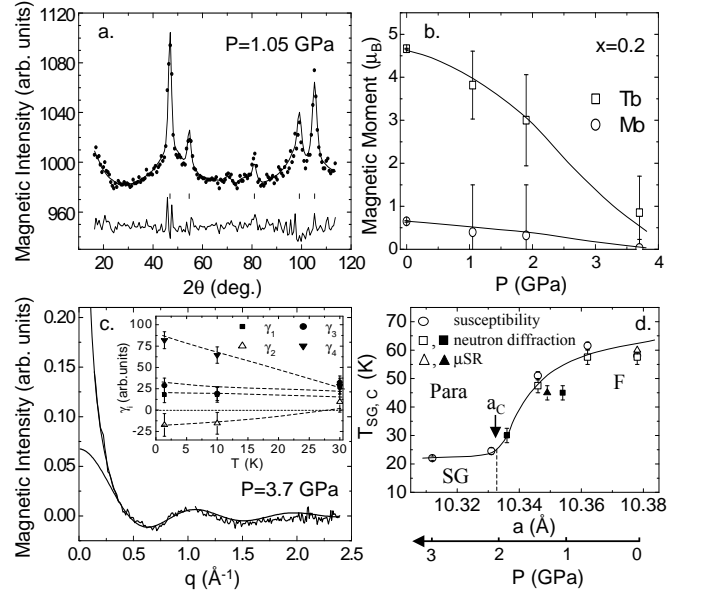


FIG. 3: a. Magnetic intensity in $x=0.2$ sample at 1.4 K and $P=1.05$ GPa, with $\Lambda=4.741$ Å. Solid lines show the best refinement ($R_B=20\%$) and the difference spectrum; b. Magnetic moment versus pressure; c. Magnetic intensity of $x=0.2$ at 1.4 K and $P=3.7$ GPa versus scattering vector. The fit is made with the short range model (bottom line), including longer range F correlations (upper line). In inset the temperature dependence of the correlations coefficients; d. phase diagram for $(\text{Tb}_{1-x}\text{La}_x)_2\text{Mo}_2\text{O}_7$ in the threshold region. Open symbols are measured at ambient pressure for several x contents. Full symbols are for $x=0.2$ under pressure, taking into account ESRF data to determine $a(P)$.

cally ordered state of a powder sample¹⁸. The first term of function below corresponds to the depolarization by spin fluctuations perpendicular to the direction of the muon spin, whereas the second term reflects the precession of the muon spin in the average local field $\langle B_{loc} \rangle$ at the muon site. The transverse relaxation rate λ_T could have both static and dynamical character. Both expressions of $P_Z(t)$ are expected to merge in the high temperature limit, when the dynamics of Tb^{3+} and Mo^{4+} moments is fast, yielding $\lambda_Z = \lambda_T$, $\langle B_{loc} \rangle = 0$ and $\beta=1$. One should also mention that a fit with a dynamical Kubo-Toyabe (DKT) depolarization function is possible for a small temperature range below T_C , but the function below gives better results at low temperature and close to T_C .

The longitudinal relaxation rate λ_Z clearly shows a cusp at $T_C \sim 60$ K. Surprisingly, with decreasing T further, λ_Z does not keep decreasing but starts to increase again below about 50 K, showing a broad maximum at $T^* \sim 25$ K. The behavior around T^* is clearly non-critical as $\lambda_Z(T)$ does not tend to diverge. The transverse relaxation rate λ_T is about 10 times larger than $\lambda_Z(T)$. It smoothly increases below T_C and scales with the average local field $\langle B_{loc} \rangle$ as temperature varies. This leads us to assign λ_T mainly to the width of the distribution

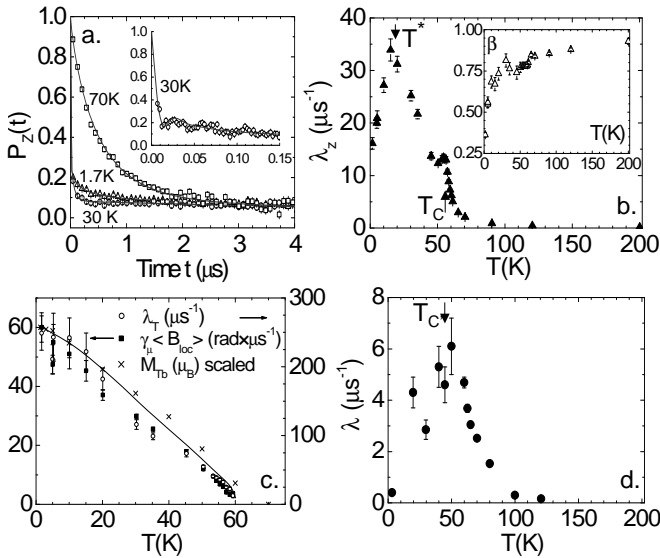


FIG. 4: μ SR results for $x=0.2$. a. Muon depolarization function $P_Z(t)$ at ambient pressure for several temperatures; b. Temperature dependence of λ_Z and β at ambient pressure; c. $\langle B_{loc} \rangle$, λ_T , and M_{Tb} (scaled) at ambient pressure; d. λ at $P=1.3$ GPa.

of local fields. Interestingly both quantities also scale with the ordered moment $M_{Tb}(T)$ measured by neutron diffraction. It suggests that the local field seen by the muon mostly comes from the Tb^{3+} ions with much larger moments, although more localized, than the Mo^{4+} ones. Previous μ SR data in spin glasses⁷ support this interpretation, showing that the static internal field is about 10 times larger in $Tb_2Mo_2O_7$ (0.7 T) than in $Y_2Mo_2O_7$ (0.066 T).

Under pressure and for temperatures below T_C it was difficult to extract any information from the μ SR spectra at small times (the 2/3 term), due both to the large back-

ground of the pressure-cell and to the fast depolarization of the 2/3 term. Therefore, below T_C , we fitted only the 1/3 term, with an exponential depolarization function, skipping the first 0.2 μ s of the μ SR spectra. There is no anomaly corresponding to T^* , suggesting that the temperatures T_C and T^* merge with increasing pressure, as the sample enters in the spin glass-like state. The fitted values of λ are clearly lower under applied pressure.

The second transition at T^* seen by μ SR recalls observations in disordered frustrated ferromagnets called reentrant spin glasses (RSG)^{19,20}. In RSG's, AF interaction compete with dominant F interactions, leading to spin glass-like anomalies below T_C . The second transition was assigned to the freezing of spin components transverse to the domain magnetization without breaking off long range ferromagnetic order, as predicted by mean field theory²¹. Here the physical meaning of T^* should be more complex since the long range magnetic order involves canted moments. We notice that there is no change in this order at T^* , as could be seen by an anomaly in the ordered moments or canting angles. We suggest a freezing of short range correlated moments below T^* since we observe diffuse scattering down to the lowest temperature. We could check it in future by inelastic neutron scattering.

In conclusion, we studied for the first time the microscopic magnetic properties at the F-SG threshold. Using pressure, we prove the dominant role of Mo-Mo distances and clarify the role of R magnetism. We also observe a new dynamical transition on the ferromagnetic side of the threshold.

We thank A. Amato and U. Zimmermann for μ SR measurements on GPS and GPD (PSI), W. Crichton for X ray measurements on ID27 (ESRF), F. Bourée and G. André for neutron measurements on 3T2 and G41 (LLB), A. Forget and D. Colson for the sample preparation (SPEC).

- ¹ S. T. Bramwell and M. J. P. Gingras, *Science* **294**, 1495 (2001).
- ² J. E. Greedan, *J. Mater. Chem.* **11**, 37 (2001).
- ³ T. Katsufuji *et al.*, *Phys. Rev. Lett.* **84**, 1998 (2000).
- ⁴ Y. Moritomo *et al.*, *Phys. Rev. B* **63**, 144425 (2001).
- ⁵ J. S. Kang *et al.*, *Phys. Rev. B* **65**, 224422 (2002).
- ⁶ I. V. Solovyev, *Phys. Rev. B* **67**, 174406 (2003).
- ⁷ S. R. Dunsiger *et al.*, *Phys. Rev. B* **54**, 9019 (1996).
- ⁸ J. E. Greedan *et al.*, *Phys. Rev. B* **43**, 5682 (1991).
- ⁹ B. D. Gaulin *et al.*, *Phys. Rev. Lett.* **69**, 3244 (1992).
- ¹⁰ J. S. Gardner *et al.*, *Phys. Rev. Lett.* **83**, 211 (1999).
- ¹¹ Y. Yasui *et al.*, *J. Phys. Soc. Jpn.* **70**, 284 (2001).
- ¹² Y. Taguchi *et al.*, *Science* **291**, 2573 (2001).
- ¹³ J. Rodríguez-Carvajal, *Physica B* **192**, 55 (1993).

- ¹⁴ I. Goncharenko, *High Pressure Research* **24**, 193 (2004).
- ¹⁵ J. Rodríguez-Carvajal, BasIreps, URL <ftp://ftp.cea.fr/pub/llb/divers/BasIreps>.
- ¹⁶ Y. A. Izyumov *et al.*, *Neutron diffraction on magnetic materials* (Consultants Bureau, New York, 1991).
- ¹⁷ I. Mirebeau *et al.*, *Phys. Rev. Lett.* **94**, 246402 (2005).
- ¹⁸ P. Dalmas de Réotier, P. C. M. Gubbens and A. Yaouanc, *J. Phys. Condens. Matter.* **16**, S4687 (2004).
- ¹⁹ I. Mirebeau *et al.*, *Hyp. Int.* **104**, 343 (1997).
- ²⁰ D. H. Ryan *et al.*, *Phys. Rev. B* **61**, 6816. (2000); *J. Phys. Condens. Matter* **16**, S4619, (2004).
- ²¹ M. Gabay and G. Toulouse, *Phys. Rev. Lett.* **47**, 201 (1981).